Nickel catalysts supported on calcium titanate for enhanced CO methanation

Chunmiao Jia,[1,2] Jiajian Gao,[1] Jing Li,[1] Fangna Gu,[1,*]
Guangwen Xu,[1] Ziyi Zhong,[3] and Fabing Su[1,*]

[1] *State Key Laboratory of Multiphase Complex Systems, Institute of Process Engineering, Chinese Academy of Sciences, Beijing, China 100190*

[2] *Graduate University of Chinese Academy of Sciences, Beijing, China 100049*

[3] *Institute of Chemical Engineering and Sciences, A*star, 1 Pesek Road, Jurong Island, Singapore 627833*

*Corresponding author: fngu@mail.ipe.ac.cn (F. Gu); fbsu@mail.ipe.ac.cn (F. Su), Tel: +86-10-82544850; Fax: +86-10-82544851

Abstract

Nickel catalysts supported on the perovskite oxide $CaTiO_3$ (CTO) were prepared by impregnation method for CO methanation to produce the synthetic natural gas (SNG). X-Ray diffraction, Nitrogen adsorption, scanning electron microscopy, transmission electron microscopy, thermogravimetric analysis, H_2-temperature programmed reduction and desorption, and X-Ray photoelectron spectroscope were employed for the characterization of samples. The results revealed that the Ni/CTO catalysts showed better performance than Ni/Al_2O_3 for CO methanation at different reaction conditions. The life time test at 600 ^oC and 3.0 MPa indicates the Ni/CTO is also more active, thermally stable, and resistant to carbon deposition. This is because of the relatively weak Ni-CTO support interaction, highly stable CTO support, the absence of acidic sites on the surface of CTO, and the proper Ni particle size. The work is important to the development of effective methanation catalysts for SNG production.

Key words: perovskite oxide, Ni catalyst, CO methanation, Al_2O_3, carbon deposition

1. Introduction

Recently, methanation of carbon oxides (CO and/or CO_2) to produce synthetic natural gas (SNG) has drawn intensive attention due to the increasing demand for natural gas and reducing emission of greenhouse gases to atmosphere.[1] The basic reactions in the methanation process are highly exothermic, which are shown as follows: (1) $CO+3H_2 \rightarrow CH_4+H_2O$, $\Delta H_{298K} = -206.1\ kJ\cdot mol^{-1}$ and (2) $CO_2+4H_2 \rightarrow CH_4+2H_2O$, $\Delta H_{298K} = -165.0\ kJ\cdot mol^{-1}$.[2,3] Compared to the noble metal catalysts, Ni-based catalysts are very attractive and promising due to their relatively high activity, low cost and good availability. Different materials including Al_2O_3, SiC,[4] SiO_2[5] or CeO_2[6] have been used to support Ni particles, and among which, Al_2O_3 is the most widely used to produce the methanation catalyst.[7] The major drawbacks of Ni/Al_2O_3 catalyst, as pointed out previously by some researchers, include sintering of Al_2O_3 and formation of coke on Ni during the methanation process.[8,9] To overcome these limits, great efforts have been made to modify the Ni/Al_2O_3 catalysts, e.g., modification of Al_2O_3 support and use of various synthesis methods, together with the multiple promoters.[10-14] Very recently, Ni/Al_2O_3 catalyst with high Ni loadings (40 and 50 wt%) prepared by the solution combustion method was found to be stable during a 50 h test, while that with lower Ni loadings of 10–30 wt% deactivated gradually.[15] The factors leading to the deactivation of Ni/Al_2O_3 catalyst include the sintering of the Al_2O_3 support, the generation of $NiAl_2O_4$ spinel, as well as the severe coke formation.[16,17] In other words, although the above catalysts are promising for industrial production, their thermal stability and resistance to carbon deposition are still the challenge.

It has been known that perovskite oxides possesses some interesting physical and chemical properties, e. g., high thermal stability, and good reactivity of lattice oxygen, low cost, and rich resource. As catalysts or supports, perovskite oxides have been widely used in a number of high temperature reactions[18], such as steam reforming of methane,[19] CO_2 methanation,[20] selective CO oxidation reaction,[21] partial oxidation of CH_4.[22] Hayakawa *et al*.[19] reported that in steam reforming reaction of methane, the Ni/perovskite catalysts exhibited higher catalytic activities and superior coking resistance compared to the conventional Ni/α-Al_2O_3 catalyst. This is because the utilization of the lattice oxygen in the perovskite-supported catalysts was able to inhibit the formation of carbon during the reaction process. Further, Takehira and coworkers[23] evaluated the perovskite oxides $XTiO_3$ (X= Ca, Sr, Ba) containing a small Ni in the Ti sites, and these catalysts showed high catalytic activities with high resistance to coking because of their unique structure and the high dispersion of Ni. They also consider that it was the perovskite structure to separate NiO and then Ni metal consequently. However, the perovskite oxide-supported Ni catalysts have not been explored for the CO methanation reaction.

In this paper, we used $CaTiO_3$ (CTO), one of the perovskite oxides, to prepare Ni catalysts (Ni/CTO) with low NiO loadings for CO methanation for the production of SNG and found that Ni/CTO catalysts exhibit better catalytic activity, superior thermal stability, and greater resistance to coke formation comparing with Ni/Al_2O_3 catalysts, suggesting that CTO would be a good alternative material to substitute for the conventional Al_2O_3 support. Our work is significant to the development of effective CO methanation catalysts for SNG production.

2. Experimental

2.1. Catalyst preparation

All the catalysts were prepared by the wet impregnation method. Commercial perovskite CTO (NanTong AoXin Machineryco., Ltd., Purity > 95%) was calcined at 400 ^{o}C for 4 h before use. A

1.945 g of $Ni(NO_3)_2 \cdot 6H_2O$ (analytical-grade, Sinopharm Chemical Reagent Co. Ltd.) was dissolved in 13 mL of deionized water and 4.50 g CTO support was added to form a slurry, which was kept at room temperature for 8 h under vigorous stirring. Then the slurry was heated to 80 ^{o}C to evaporate the liquid, then dried at 110 ^{o}C overnight, and further calcined at 400 ^{o}C for 4 h in air. The collected catalyst was denoted as 10Ni/CTO with a NiO loading of 10 wt %. Accordingly, 5Ni/CTO was prepared by the same method using 0.973 g $Ni(NO_3)_2 \cdot 6H_2O$, 4.75 g CTO and 15 mL deionized water. For a comparison, commercial γ-Al_2O_3 (GongYiHuaYu alumina Co. Ltd., China; Purity> 95%) was also calcined at 400 ^{o}C in air for 4 h before use, and the 5Ni/Al_2O_3 and 10Ni/Al_2O_3 catalysts were prepared by the same method.

2.2. Characterization

The X-ray powder diffraction (XRD) pattern was recorded on a PANalytical X'Pert PRO MPD with the Kα radiation of Cu (λ = 1.5418 Å) at 40 KV and 40 mA, and Debye-Scherrer equation was used to calculate the crystal size. The specific surface area of the catalysts was measured on Quantachrome surface area & pore size analyzer NOVA 3200e. Before measurement, the sample was degassed at 200 ^{o}C for 3 h under vacuum. The specific surface area was determined according to the Brunauer-Emmett-Teller (BET) method in the relative pressure range of 0.05–0.2. The microscopic feature of the samples was observed by field emission scanning electron microscope (SEM) (JSM-6700F, JEOL, Tokyo, Japan) and transmission electron microscopy (TEM) (JEM-2010F, JEOL, Tokyo, Japan). Prior to the TEM observation, the catalyst was first reduced in a continuous-flow fixed bed at 600 ^{o}C for 4 h under H_2 with the flow rate of 50 $mL \cdot min^{-1}$. Thermal gravimetric analysis was conducted on a Seiko Instruments EXSTAR TG/DTA 6300. 10 mg of the sample was used and heated under air (200 $mL \cdot min^{-1}$) from room temperature up to 1000 ºC (10

^{o}C·min^{-1}). The surface chemical composition was analyzed by X-Ray photoelectron spectroscopy (XPS) test was conducted on a VG ESCALAB 250 spectrometer (Thermo Electron, U.K.) with a non-monochromatized Al Kα X-Ray source (1486 eV). The deposited carbon content was measured using CS-344 Infrared Analyzer (Leco, US). H_2 temperature-programmed reduction (H_2-TPR) and desorption (H_2-TPD), and NH_3 temperature-programmed desorption (NH_3-TPD) were carried out on Quantachrome Automated chemisorption analyzer (ChemBET pulsar TPR/TPD). The H_2 consumption or NH_3 desorption was detected continuously as a function of increasing temperature using a thermal conductivity detector (TCD). For H_2-TPR test, 0.1 g of the sample was loaded in a quartz U-tube and heated from room temperature to 400 ^{o}C with 10 ^{o}C·min^{-1} and maintained for 1 h under Ar flow. Then, the sample was cooled to room temperature and followed by heating to 1000 ^{o}C with 10 ^{o}C·min^{-1} under a 10.0 vol % H_2/Ar with a gas flow of 30 mL·min^{-1}. For NH_3-TPD, 0.3 g of the sample was loaded in a quartz U-tube and reduced from room temperature to 600 ^{o}C according to the H_2-TPR procedure, then the gas flow was switched to He flow (30 mL·min^{-1}) and the sample was cooled to 100 ^{o}C and saturated with ammonia (10.0 vol % NH_3/He). After removing the physically adsorbed ammonia in He flow for 1 h, the sample was heated to 600 ^{o}C at 10 ^{o}C·min^{-1} in He flow. For H_2-TPD, 0.3 g catalyst was loaded into a quartz U-tube and firstly reduced at 600 ^{o}C for 4 h under a 10.0 vol % H_2/Ar with a gas flow of 30 mL·min^{-1}, then cooled to room temperature and kept for 2 h. After removing the physically adsorbed hydrogen by flush with Ar for 2 h at the flow rate of 30 mL·min^{-1}, the sample was heated to 600 ^{o}C ramping with a ramp of 10 ^{o}C·min^{-1} in Ar flow. The number of surface Ni sites per unit mass of catalyst is determined by means of H_2-TPD with adsorption stoichiometry of H/Ni = 1:1. The peak area of H_2-TPD profile was normalized by that of H_2-TPR of a standard CuO sample. The turnover frequency (TOF) value is calculated based on the formula as followed:

$$\mathbf{TOF}_{\mathbf{CO}} = \frac{V_{\mathbf{CO,in}} - V_{\mathbf{CO,out}}}{R_{\mathbf{H_2/Ni}} * V_m} * \frac{m_{\mathbf{cat\text{-}TPD}}}{m_{\mathbf{cat\text{-}Reaction}}} * \frac{A_{\mathbf{CuO\text{-}TPR}}}{A_{\mathbf{cat\text{-}TPD}}} * \frac{\mathbf{M}_{\mathbf{CuO}}}{m_{\mathbf{CuO\text{-}TPR}}}$$

$V_{\mathbf{CO,in}}$ and $V_{\mathbf{CO,out}}$, the volume flow rate of CO at the inlet and outlet of the reactor at standard temperature and pressure (STP), mL·s^{-1};

$R_{\mathbf{H_2/Ni}} = 2$, stoichiometric factor of the H_2:Ni ratio in the chemisorption;

$V_m = 22414$ mL·mol^{-1}, molar volume of CO gas at STP;

$m_{\mathbf{cat\text{-}TPD}}$, the mass of the catalysts used in the H_2-TPD experiment, g;

$m_{\mathbf{cat\text{-}Reaction}}$, the mass of the catalysts used in the CO methanation reaction, g;

$A_{\mathbf{CuO\text{-}TPR}}$, the peak area of the H_2-TPR cure of standard CuO;

$A_{\mathbf{cat\text{-}TPD}}$, the peak area of the H_2-TPD cure of the catalyst;

$\mathbf{M}_{\mathbf{CuO}} = 79.54$ g·mol^{-1}, the mole mass of CuO;

$m_{\mathbf{CuO\text{-}TPR}}$, the mass of the CuO used in the H_2-TPR experiment, g.

2.3. Catalytic Measurement

The catalytic tests for CO and CO_2 methanation were carried out in a fixed-bed reactor equipped with quartz tube and stainless steel tube (both with a diameter of 8 mm) respectively. A thermocouple was inserted into the furnace chamber and bonded the outside of the reactor tube in the middle of catalyst bed to control the reaction temperature. The CO methanation was tested under 0.1 and 3.0 MPa from 300 to 600 ^{o}C, and CO_2 methanation was also performed under 0.1 MPa. 0.6 g of catalyst (20–40 mesh) diluted with 3.0 g of quartz sand of the same mesh was placed in the tube reactor. The catalyst was firstly reduced at 600 ^{o}C for 4 h under pure H_2 flow (100 mL·min^{-1}), then the gas flow was switched to the feed gas with a molar ratio of $H_2/CO/N_2 = 3/1/1$, and the total flow rate was set to 100 mL·min^{-1} determined by mass flow controllers corresponding to the weight hourly space velocity (WHSV) of 10,000 mL·g^{-1}·h^{-1}. Heating the mixture from 300 to 600 ^{o}C with an interval of 50 ^{o}C, the catalytic activities of the catalysts were measured under 0.1 and 3.0 MPa respectively. Life time test was performed at 600 ^{o}C and 3.0 MPa. For hydrothermal treatment, 0.5 g of the unreduced catalyst was loaded into a quartz tube, and subjected to an atmosphere of steam and hydrogen with a volume ratio of 10 : 1 at 800 ^{o}C for 5 hours under 0.1 MPa, and then the catalyst was cooled to room temperature in pure H_2. For CO_2 methanation, feed gas with a molar ratio of $H_2/CO_2/N_2$ = 4/1/1 was used. The inlet and outlet gas after cooled using cold trap were analyzed on line by Micro GC (3000A; Agilent Technologies). After one hour of steady-state operation at each temperature, the concentrations of H_2, N_2, CH_4, CO and CO_2 contents in gas products were analyzed by a thermal conductivity detector (TCD) with a Molecular Sieve column using N_2 as an internal standard.

CO and CO_2 conversion, CH_4 selectivity and yield are defined as follows:

$$X_i\ (\%) = \frac{F_{i,\mathrm{in}} - F_{i,\mathrm{out}}}{F_{i,\mathrm{in}}} \times 100 \tag{1}$$

$$S_{\mathrm{CH_4}}\ (\%) = \frac{F_{\mathrm{CH_4,out}}}{F_{i,\mathrm{in}} - F_{i,\mathrm{out}}} \times 100 \tag{2}$$

$$Y_{\mathrm{CH_4}}\ (\%) = \frac{X_i \cdot S_{\mathrm{CH_4}}}{100} = \frac{F_{\mathrm{CH_4,out}}}{F_{i,\mathrm{in}}} \times 100 \tag{3}$$

Here, i represents CO or CO_2, X is the conversion of CO or CO_2, S is the selectivity of CH_4, Y is the CH_4 yield, $F_{x,in}$ and $F_{x,out}$ are molar flow rate of species x (x = CH_4, CO, or CO_2) at inlet and outlet respectively.

3. Results and Discussion

3.1. Catalyst characterization

Table 1 compiles the surface areas and pore volumes of the supports and catalysts. CTO has a very low surface area (1.6 $m^2 \cdot g^{-1}$) and is almost non-porous. After NiO loading, the surface area of the CTO supported catalysts increase slightly. This can be attributed to the loading of small NiO nanoparticles on the surface of CTO, which can be seen from SEM images below. While for Al_2O_3 and Ni/Al_2O_3 catalysts, their surface areas (246–305 $m^2 \cdot g^{-1}$) and total pore volumes (0.34–0.44 $m^3 \cdot g^{-1}$) are much larger than those of CTO and Ni/CTO catalysts, but become smaller after the NiO loading, mainly because the density of the NiO particles is larger than that of the porous Al_2O_3 and some of the pores may be blocked by NiO nanoparticles.

Figure 1 presents the XRD patterns and TG curves of the calcined catalysts and the support. For the Ni/CTO samples in Figure 1a, the diffraction peaks at 33.3, 47.9, 59.6, and 70.0^o are the typical feature of CTO.[23,24] From the enlarged view zone in Figure 1b, the peaks at 37.4, 43.5, and 63.2^o can be attributed to (111), (200), and (220) of NiO (JCPDS 00-001-1239).[25] As expected, with the increase of the NiO loading from 5 to 10 wt%, the intensities of these peaks are increased obviously, indicating the formation of larger NiO particles. The sizes of NiO on 5Ni/CTO and 10Ni/CTO are calculated to be 19 and 24 nm, respectively (see Table 1). The XRD patterns of the Al_2O_3 support and Ni/Al_2O_3 catalysts are depicted in Figure 1c, in which an extremely weak diffraction peak at 43.3^o contributed to NiO is detected, indicating the low NiO loading or high dispersion.[26] Figure 1d shows the TG/DTA curves of the two supports. Clearly, CTO experiences a weight loss of less than 0.5 wt% at 1000 ^oC, much lower than that of the Al_2O_3 (~5 wt%), suggesting the superior thermal stability of CTO to Al_2O_3.[27,28]

Figure 2 shows the H_2-TPR, H_2-TPD, and NH_3-TPD curves of the supports and the Ni catalysts. From Figure 2a, it can be seen that there is no obvious reduction peak for both the CTO and Al_2O_3 supports, implying that they are non-reducible under this condition. The reducible NiO peaks of the catalysts can be approximately classified into three types: α-type (weak interaction of the NiO and support, 290–475 ^{o}C), β-type (mid-interaction, 475–753 ^{o}C), and γ-type (strong interaction, 753–894 ^{o}C). [,15,29] The H_2 consumption curves of the Ni catalysts are fitted by Gaussian-type functions and the quantitative results are listed in Table 2. Accordingly, we can see the reducible NiO peak in 10Ni/CTO samples is located in the range of 295–471 ^{o}C, and all belongs to the reduction of α-type NiO i.e. free Ni which interacts weakly with CTO support, and the 5Ni/CTO catalyst possesses the same type NiO (reducible peak from 311 to 471 ^{o}C). In contrast, for the Ni/Al_2O_3 catalysts, both the reducible peaks include three sub-peaks corresponding to α-type, β-type, and γ-type. Particularly, β-type NiO becomes dominant and the fraction increases with the NiO loading (42.4% for $5Ni/Al_2O_3$ to 53.5% for $10Ni/Al_2O_3$ in Table 2), and γ-type NiO is also found in both catalysts, implying NiO strongly interacts with Al_2O_3 and partly generate $NiAl_2O_4$ spinel structure, which is highly stable and hence difficult to be reduced.[25] In short, the metal-support interaction in Ni/CTO is relatively weaker than that of Ni/Al_2O_3. The surface acidic properties of the supports and catalysts are examined by NH_3-TPD as shown in Figure 2b. There is no any desorption peak of ammonia on both CTO and 10Ni/CTO in the temperature range of 100–600 ^{o}C, indicating the lack of acidic sites on their surface. In contrast, a broad desorption peak is observed over the Al_2O_3 and $10Ni/Al_2O_3$ in the range of 150–450 ^{o}C, which can be attributed to the desorbed NH_3 from acid site.[30,31] In short, the surface of 10Ni/CTO possesses non-acidic nature while that of $10Ni/Al_2O_3$ shows relatively strong acidic property. Figure 2c shows the H_2-TPD curves of the reduced catalysts. We can see that the TPD profiles show H_2 desorption peaks in the range of 50–360 ^oC for both catalysts, and H_2 adsorption amount for 10Ni/Al_2O_3 catalyst is 14.6 μmol/g_{cat}, much higher than that of 10Ni/CTO catalyst (5.0 μmol/g_{cat}), possibly because smaller Ni particles are dispersed well on Al_2O_3 support due to its high surface area and intricate pore structure.

Figure 3 presents the SEM images of the supports and the unreduced catalysts. Figure 3a shows that the CTO support possesses a smooth surface. For 5Ni/CTO (Figure 3c) and 10Ni/CTO (Figure 3e), it is seen that the NiO particles are uniformly dispersed on CTO surface. Furthermore, the NiO particle size in 10Ni/CTO appears slightly larger than that in 5Ni/CTO, in agreement with the XRD results (Figure 1). In contrast, the Al_2O_3 support itself is consisted of small particles (Figure 3b). After loaded with NiO, no visible change can be seen in 5Ni/Al_2O_3 (Figure 3d) and 10Ni/Al_2O_3 (Figure 3f). All the SEM images indicate that the NiO particles are well dispersed on the surface of CTO and Al_2O_3 supports.

Figure 4 shows the TEM images of the reduced Ni catalysts. The Ni particles are well dispersed on the CTO support surface (5Ni/CTO in Figure 4a and 10Ni/CTO in Figure 4c). The Ni particle sizes in 5Ni/CTO and in 10Ni/CTO are about 10–20 nm and 20–30 nm, respectively. Figure 4e shows that smaller Ni particles (5–10 nm) are dispersed on the Al_2O_3 support. In addition, Figure 4b, 4d, and 4f show the HRTEM images of the Ni particles with the exposed Ni lattice space of 0.2 nm, corresponding to Ni(111) space, which is the active face for methanation.[11,32]

Figure 5 displays the XPS spectra of Ni 2p and O 1s, and Table 3 lists the data for other elements of supports. The XPS spectra of all the samples confirm that expected elements (Ni, Ca, Ti, Al and O) are presented in Ni/CTO and Ni/Al_2O_3. The surface of the Ni/CTO catalysts are covered by a small portion of metal Ni (Ni $2p_{3/2}$ at around 853.0 eV) and a larger portion of Ni oxide (Ni $2p_{3/2}$ at around 856.4 eV), due to the partial surface oxidation of Ni during the sample transfer before XPS test.[33,34] Moreover, the Ni $2p_{3/2}$ peak of 10Ni/CTO shifts to a lower binding energy of 852.3 eV compared with that of 5Ni/CTO (856.4 eV), indicating that the interaction of Ni particles with the CTO support become weaker as the loading amount of Ni increases. For the 10Ni/Al_2O_3 catalyst, two peaks at 856.4 and 874.0 eV, which are assigned to NiO $2p_{3/2}$ and NiO $2p_{1/2}$ respectively, are observed; meanwhile, no obvious signal of metal Ni is identified.[35] The absence of reduced Ni phase in 10Ni/Al_2O_3 catalyst is likely attributed to the oxidation of metallic Ni after exposure to air, because the catalysts were not reduced again in situ during the XPS measurement. Additionally, the formation of highly stable $NiAl_2O_4$ phase also account for this phenomenon.[35] The O 1s signals in Figure 5b for Ni/CTO catalysts can be fitted to two peaks around 530.0 and 532.0 eV, respectively. With the increase of the NiO loading, the proportion of O in NiO (530.0 eV) increases compared with O in CTO (532.0 eV).[36,37] 10Ni/Al_2O_3 has a broader O 1s peak, which can be fitted with three sub-peaks corresponding to three types O on NiO (529.8 eV), Al_2O_3 (531.0 eV) and as well as $NiAl_2O_4$ (532.0 eV) because of the strong interaction between Ni and support Al_2O_3, respectively.[35,38,39] Apart from these, the binding energy of the other elements (Ca $2p_{3/2}$, Ca $2p_{1/2}$, Ti $2p_{3/2}$, Ti $2p_{1/2}$, and Al 2p) have no obvious chemical shift, implying that the chemical environment of the both supports may not be changed after Ni loaded.[40]

3.2. Catalyst activity

Figure 6 shows the activities of the Ni catalysts for CO methanation at 0.1 MPa. Overall, the CO conversion and CH_4 yield over the Ni/CTO catalysts present a volcano-shaped trend as the reaction temperature changes, agreement with the thermodynamic calculation.[3] The CO conversion in Figure

6a almost reaches 100% over 10Ni/CTO at 400 ^oC, while over 5Ni/CTO it needs a higher reaction temperature of 450 ^oC for reaching the same CO conversion. At the same time, the maximum CO conversion over 10Ni/Al_2O_3 is only 28% at 600 ^oC, and that over 5Ni/Al_2O_3 catalyst is even lower (8%) at 500 ^oC. The maximum CH_4 selectivity for 10Ni/CTO and 5Ni/CTO catalysts is 85% at 400 ^oC and 80% at 450 ^oC in Figure 6b, respectively. In addition, the maxima of CH_4 selectivity over 10Ni/Al_2O_3 and 5Ni/Al_2O_3 are around 80% and 88% respectively. From Figure 6c, the maximum CH_4 yield on 10Ni/CTO is 84% at 400 ^oC, and 80% on 5Ni/CTO at 450 ^oC. Meanwhile, the max CH_4 yields on 10Ni/Al_2O_3 and 5Ni/Al_2O_3 samples are just 24% and 6%, respectively. In order to further confirm the superiority of 10Ni/CTO catalyst, the TOF values were calculated based on the H_2-TPD and CO conversion results at 400 ^oC. The TOF_{CO} value over 10Ni/CTO is 2.4 s^{-1}, 24 times of that over 10Ni/Al_2O_3 catalysts (0.1 s^{-1}), indicating the catalytic efficiency on reduced 10Ni/CTO is significantly higher than that of 10Ni/Al_2O_3. In addition, we tried to completely reduce both catalysts at 800 ^oC for 4 h in pure H_2, and found that CO conversion and CH_4 yield over 10Ni/Al_2O_3 are still much lower than that on 10Ni/CTO at 0.1 MPa and 120,000 $mL\cdot g^{-1}\cdot h^{-1}$ (data not shown here).Therefore, we can deduce the 10Ni/CTO is more active than 10Ni/Al_2O_3 catalyst.

Previously, a great deal of efforts have been made to understand the interaction between the metal component and the support, and the strong metal support interaction (SMSI) was often used to explain experimental phenomena.[4,36,41,42] However, above characterization results demonstrate that the Ni/CTO catalysts have weaker metal-support interactions compared with the Ni/Al_2O_3 catalysts, but they show better catalytic performance. Thus, the SMSI model is not appropriate to explain the above phenomena. Therefore, we may suspect that the NiO strongly interacted with the support may not be fully available in the catalytic reaction, because part of them is difficult to be reduced to act the “active” role. This is what has occurred in Ni/Al_2O_3 although it has a high dispersion of Ni nanoparticles. In order to fully reduce the NiO species in this catalyst, a higher reduction temperature is needed, which will adversely lead to the agglomeration of Ni particles and support, and the formation of $NiAl_2O_4$.[35] These may not be helpful for improving the catalytic activity for Ni/Al_2O_3. Contrarily, in the Ni/CTO catalysts, even at the low reduction temperature of 600 ^{o}C all NiO can be reduced, which leads to a full utilization of Ni species and minimum impact to the sintering of Ni and support. We thus can consider that a weak interaction in the Ni/CTO catalysts is responsible for its good catalytic performances.

Figure 7 shows the catalytic properties of CO methanation under 3.0 MPa over the 10Ni/CTO and $10Ni/Al_2O_3$ catalysts. As we know that this reaction is volume-reduced and normally conducted at high pressure (2.94–3.43 MPa) in industry.[43] It is seen that the CO conversion (Figure 7a) over the 10Ni/CTO catalyst reaches almost 100% and maintains constant from 350 to 600 ^{o}C. However, the CO conversion over the $10Ni/Al_2O_3$ catalyst increases with heating up and only reaches 73% at the temperature of 600 ^{o}C. It can be seen that the CH_4 selectivity (Figure 7b) on 10Ni/CTO maintains between 80 to 90% during the whole temperature range, while that on $10Ni/Al_2O_3$ reaches the maximum 60% at 600 ^{o}C. In Figure 7c, maximum value of CH_4 yield on 10Ni/CTO is around 88% from 450 to 600 ^{o}C, but it is only 45% for $10Ni/Al_2O_3$ sample at 600 ^{o}C. In addition, the thermodynamic equilibrium data is included for a comparison. It can be seen that the CO conversion on 10Ni/CTO catalyst almost reaches the thermodynamic equilibrium value above 600 ^{o}C and there is a large difference for $10Ni/Al_2O_3$. For CH_4 selectivity and yield, the gap between experiment and thermodynamic equilibrium can be seen, especially over $10Ni/Al_2O_3$. Therefore, the results in high pressure test still indicate that 10Ni/CTO catalyst is more active than

10Ni/Al_2O_3.

Figure 8 shows the life time test results of 10Ni/CTO and 10Ni/Al_2O_3 at 600 ^oC and 3.0 MPa. For 10Ni/CTO catalyst, CO conversion (Figure 8a), CH_4 selectivity (Figure 8b), and CH_4 yield (Figure 8c) is ~100, ~84, and ~83%, respectively, and these retain constant during 50 h run. In contrast, the activity of the 10Ni/Al_2O_3 catalyst has remarkable decline only after 20 h, for instance, the CO conversion from 70 to 45%, and CH_4 yield from 41to 18%, suggesting the better long term performance of 10Ni/CTO.

Figure 9a shows the XRD pattern of the used 10Ni/Al_2O_3 catalyst after 20 h test and freshly reduced catalyst for comparison. In the reduced catalyst, there is no metallic Ni peaks identified, but after the long life time test, the Ni peaks located at 44.8, 51.9, and 76.6^o appear obviously and the Ni particle size is calculated to be about 26 nm, suggesting the sintering and agglomeration of Ni particles after the long term methanation.[25] However, for 10Ni/CTO catalyst in Figure 9b, no obvious change is observed referencing the reduced and used catalyst after the 50 h reaction, indicating its good stability. Figure 9c shows the SEM image of 10Ni/Al_2O_3 catalyst after 20 h test. It is seen that there are some filamentous carbons formed, suggesting the carbon deposition occurred on the surface 10Ni/Al_2O_3, consistent with previous results.[26] In contrast, for the 10Ni/CTO catalyst in Figure 9d, no such carbon filaments can be found even after 50 h reaction. The amount of carbon deposited on the 10Ni/CTO after 50 h test and 10Ni/Al_2O_3 after 20 h analyzed by CS-344 Infrared Analyzer is 1.4 and 1.6 wt%, and the average carbon deposition rate is 0.03 and 0.08 $wt\%\cdot h^{-1}$, respectively, suggesting much stronger resistance to carbon deposition for 10Ni/CTO. It has been pointed out that coking and sintering are the main factors for deactivation of metal nanoparticles, and the Ni-based catalyst is more susceptive to the deposited carbon than other active components during the methanation process.[1,9,44,45] In the CO methanation process, the carbon deposition mainly comes from the Boudouard reaction ($2CO \leftrightarrow C + CO_2$), carbon monoxide reduction ($CO + H_2 \leftrightarrow C + H_2O$) and methane cracking ($CH_4 \leftrightarrow C + 2H_2$).[8] According to the thermodynamic analysis,[3] most carbon comes from the Boudouard reaction because its equilibrium constant (K) is much larger than that of other reactions. It should be pointed out that, differing from the literature reported conditions, such as that used in removal of CO[46] and other with high H_2 content,[47,48] the feed gas ($CO/H_2/N_2$=3/1/1) used in our work is rich in carbon content, thus carbon deposition is much easier. It has been reported that carbon deposition is closely related to the surface chemistry of the active metal and the support, the dispersion and size of active metal nanoparticles, and the reaction conditions. Al_2O_3 used here is highly porous and acidic, and carbon is favorably deposited in the pores. [,49] Sintering of Al_2O_3 support at the high temperatures leads to the aggregation of Ni particles, which would exacerbate the carbon deposition. In contrast, CTO has less pores and basic surface properties, showing higher resistance to carbon deposition. In addition, the migration of mobile oxygen from the perovskite support to the metallic Ni particles in Ni/CTO[19,24,31,48] to reduce deposited carbon may be another reason.

The catalytic properties of 10Ni/CTO and 10Ni/Al_2O_3 after a HT treatment are shown in Figure 10. It can be seen that the maximum CO conversion and CH_4 yield over 10Ni/CTO-HT is around 65% (Figure 10a) and 45% (Figure 10b) at 550 ^oC, respectively, much higher than those of 10Ni/Al_2O_3-HT, although the activity of both catalysts declines compared with that of fresh catalysts in Figure 6. According to the XRD analysis on the catalysts after hydrothermal treatment (not shown here), the severe phase transformation of Al_2O_3 support (partly from γ-type to η-type) occurs and the Ni peaks appear as a result of aggregation of small Ni particles (size increased from about 3–5 nm to about 18 nm), while the structure of 10Ni/CTO almost is not changed and the Ni particle size is slightly larger (from 23 to 30 nm). Hence the better stability of 10Ni/CTO especially the CTO support are confirmed, which guarantee the superior catalytic activity and stability of the Ni/CTO catalysts. In industrial methanation process, steam is often added to the reaction system for the benefit of heat transmission and diminishment of deposited carbon.[51] Thus, the hydrothermal stability of the Ni catalysts is highly demanded.[52]

CO_2 methanation as another essential methanation process was also carried out over 10Ni/CTO and 10Ni/Al_2O_3 catalysts as shown in Figure 11. Apparently, the maximum CO_2 conversion over 10Ni/CTO reaches 75 % at 400 ^{o}C as shown in Figure 11a, while that over 10Ni/Al_2O_3 is only around 5 %, and it finally reaches its maximum value of 84 % at 600 ^{o}C. Figure 11b shows that the CH_4 yield over 10Ni/CTO substantially exceeds that over 10Ni/Al_2O_3 catalyst. Further, we can see the CO_2 conversion over the Ni catalysts is lower than that of CO, possibly because CO is much easier to be hydrogenated than CO_2.[3] Expectedly, for CO_2 methanation, the Ni/CTO also exhibits better activity than Ni/Al_2O_3, indicating Ni/CTO catalyst is a promising candidate not only for CO but also for CO_2 methanation to produce SNG.

As we know, the family of perovskite-type oxides has many members, including $BaTiO_3$, $SrTiO_3$, $MgTiO_3$, $LaNiO_3$, and so on. Based on the above results, CTO used as Ni catalyst support here may not be the best one. Thus, more exploration is needed to seek better perovskite oxide supports for methanation catalyst with much high activity and stability in our future work.

4. Conclusions

In this work, we report the preparation and characterization of perovskite CTO supported Ni catalyst with low NiO loadings for the CO methanation. It reveals that the Ni/CTO catalysts show better catalytic performance than Ni/Al_2O_3 at 0.1 MPa and 3.0 MPa, respectively. Nearly 100% CO conversion and 85% CH_4 selectivity can be achieved over 10Ni/CTO catalyst (NiO loading: 10 wt%) under 0.1 MPa, at a WHSV of 10,000 $mL{\cdot}g^{-1}{\cdot}h^{-1}$ and the H_2/CO feed ratio of 3. Life time test at 3.0 MPa and 600 ^{o}C demonstrates that Ni/CTO catalyst maintains its good stability after the 50 h reaction. It is found that the main factors accounting for the better catalytic activity over Ni/CTO than Ni/Al_2O_3 are the weak interaction between Ni and CTO support, proper Ni particle size (resistance to carbon deposition), the superior stability and non-acidic nature of CTO. This work demonstrates that the perovskite oxide CTO would be an appropriate Ni catalyst support for CO and CO_2 methanation process.

Acknowledgments

The authors gratefully acknowledge the supports from the Hundred Talents Program of the Chinese Academy of Sciences (CAS), State Key Laboratory of Multiphase Complex Systems of China (No. MPCS-2009-C-01), National Key Technology R&D Program of China (No. 2010BAC66B01), and National Key Basic Research Program of China (No. 2011CB200906). F. Gu is grateful to the support of K.C. Wang Post-doctoral Fellowships of the CAS and China Postdoctoral Science Foundation (No. 20100480026).

Notes and References

1 M. Vannice, *Cat. Rev. Sci. Eng.*, 1976, **14**, 153.

2 V. Ponec, *Cat. Rev. Sci. Eng.*, 1978, **18**, 151.

3 J. Gao, Y. Wang, Y. Ping, D. Hu, G. Xu, F. Gu and F. Su, *RSC Adv.*, 2012, **2**, 2358.

4 Y. Yu, G Q. Jin, Y. Y. Wang and X. Y. Guo, *Fuel Process. Technol.*, 2011, **92**, 2293.

5 Y. Wang, R. Wu and Y. Zhao, *Catal. Today*, 2010, **158**, 470.

6 S. D. Senanayake, J. Evans, S. Agnoli, L. Barrio, T. L. Chen, J. Hrbek and J. A. Rodriguez, *Top. Catal.*, 2011, **54**, 34.

7 D. Hu, J. Gao, Y. Ping, L. Jia, P. Gunawan, Z. Zhong, G. Xu, F. Gu and F. Su, *Ind. Eng. Chem. Res.*, 2012, **51**, 4875.

8 D. C. Gardner and C. H. Bartholomew, *Ind. Eng. Chem. Prod. Res. Dev.*, 1981, **20**, 80.

9 J. Gao, C. Jia, J. Li, F. Gu, G. Xu, Z. Zhong and F. Su, *Ind. Eng. Chem. Res.*, 2012, **51**, 10345.

10 K. O. Xavier, R. Sreekala, K. K. A. Rashid, K. K. M. Yusuff and B. Sen, *Catal. Today*, 1999, **49**, 17.

11 S. L. Ma, Y. S. Tan and Y. Z. Han, *J. Nat. Gas Chem.*, 2011, **20**, 435.

12 A. E. Aksoylu, A. N. Akin, S. G. Sunol and Z. I. Onsan, *TUrk. J. Chem.*, 1996, **20**, 88.

13 E. Kis, R. MarinkovicNeducin, G. Lomic, G. Boskovic, D. Z. Obadovic, J. Kiurski and P. Putanov, *Polyhedron*, 1998, **17**, 27.

14 M. V. Twigg and J. T. Richardson, *Appl. Catal., A*, 2000, **190**, 61.

15 A. Zhao, W. Ying, H. Zhang, H. Ma and D. Fang, *Catal. Commun.*, 2012, **17**, 34.

16 J. R Rostrup-Nielsen, K. Pedersen and J. Sehested, *Appl. Catal., A*, 2007, **330**, 134.

17 I. Levin and D. Brandon, *J. Am. Ceram. Soc.*, 1998, **81**, 1995.

18 M. A. Pena and J. L. G. Fierro, *Chem. Rev.*, 2001, **101**, 1981.

19 K. Urasaki, Y. Sekine, S. Kawabe, E. Kikuchi and M. Matsukata, *Appl. Catal., A*, 2005, **286**, 23.

20 J. Gao, L. Jia, W. Fang, Q. Li and H. Song, *J. Fuel Chem. Technol.*, 2009, **37**, 573.

21 R. N. S. H. Magalhaes, F. S. Toniolo, V. T. da Silva and M. Schmal, *Appl. Catal., A*, 2010, **388**, 216.

22 T. Hayakawa, H. Harihara, A. G. Andersen, K. Suzuki, H. Yasuda, T. Tsunoda, S. Hamakawa, A. P. E. York, Y. S. Yoon, M. Shimizu and K. Takehira, *Appl. Catal., A*, 1997, **149**, 391.

23 K. Takehira, T. Hayakawa, H. Harihara, A. Andersen, K. Suzuki and M. Shimizu, *Catal. Today*, 1995, **24**, 237.

24 K. Takehira, T. Shishido and M. Kondo, *J. Catal.*, 2002, **207**, 307.

25 J. M. Rynkowski, T. Paryjczak and M. Lenik, *Appl. Catal., A*, 1993, **106**, 73.

26 K. Y. Koo, H. S. Roh, Y. T. Seo, D. J. Seo, W. L. Yoon and S. Bin Park, *Int. J. Hydrogen Energy*, 2008, **33**, 2036.

27 P. Billik, M. Caplovicova, T. Turanyi, L. Caplovic and B. Horvath, *Mater. Res. Bull.*, 2011, **46**, 2135.

28 A. Duevel, E. Romanova, M. Sharifi, D. Freude, M. Wark, P. Heitjans and M. Wilkening, *J. Phys. Chem. C*, 2011, **115**, 22770.

29 J. Zhang, H. Y. Xu, X. L. Jin, Q. J. Ge and W. Z. Li, *Appl. Catal., A*, 2005, **290**, 87.

30 S. M. Kim, Y. J. Lee, J. W. Bae, H. S. Potdar and K. W. Jun, *Appl. Catal., A*, 2008, **348**, 113.

31 F. Meshkani and M. Rezaei, *Catal. Commun.*, 2011, **12**, 1046.

32 A. H. Zhang, J. Zhu and W. H. Duan, *Surf. Sci.*, 2007, **601**, 475.

33 A. Romero, M. Jobbagy, M. Laborde, G. Baronetti and N. Amadeo, *Catal. Today*, 2010, **149**, 407.

34 I. Czekaj, F. Loviat, F. Raimondi, J. Wambach, S. Biollaz and A. Wokaun, *Appl. Catal., A*,

2007, **329**, 68.

35 Z. Y. Hou, O. Yokota, T. Tanaka and T. Yashima, *Appl. Catal., A*, 2003, **253**, 381.

36 J. Escobar, J. A. De Los Reyes and T. Viveros, *Appl. Catal., A*, 2003, **253**, 151.

37 S. Holliday and A. Stanishevsky, *Surface & Coatings Technology*, 2004, **188**, 741.

38 R. B. Shalvoy, P. J. Reucroft and B. H. Davis, *J. Vac. Sci. Technol.*, 1980, **17**, 209.

39 L. Salvati, L. E. Makovsky, J. M. Stencel, F. R. Brown and D. M. Hercules, *J. Phys. Chem.*, 1981, **85**, 3700.

40 N. Perkas, G. Amirian, Z. Y. Zhong, J. Teo, Y. Gofer and A. Gedanken, *Catal. Lett.*, 2009, **130**, 455.

41 Y. J. Huang, J. A. Schwarz, J. R. Diehl and J. P. Baltrus, *Appl. Catal.*, 1988, **37**, 229.

42 S. M. Fang, J. M. White, T. J. Campione and J. G. Ekerdt, *J. Catal.*, 1985, **96**, 491.

43 P. Mondal, G. S. Dang and M. O. Garg, *Fuel Process. Technol.*, 2011, **92**, 1395.

44 K. B. Kester and J. L. Falconer, *J. Catal.*, 1984, **89**, 380.

45 J. Lu, B. Fu, M. C. Kung, G. Xiao, J. W. Elam, H. H. Kung and P. C. Stair, *Science*, 2012, **335**, 1205.

46 S. H. Kim, S.-W. Nam, T.-H. Lim and H.-I. Lee, *Appl. Catal., B*, 2008, **81**, 97.

47 S. Takenaka, T. Shimizu and K. Otsuka, *Int. J. Hydrogen Energy*, 2004, **29**, 1065.

48 P. Ðinović, C. Galletti, S. Specchia and V. Specchia, *Catal. Today*, 2011, **164**, 282.

49 F. Su, J. Zeng, P. Bai, L. Lv, P. Guo, H. Sun, H. Li, J. Yu, J. Y. Lee and X. S. Zhao, *Ind. Eng. Chem. Res.*, 2007, **46**, 9097.

50 J. H. Kim, D. J. Suh, T. J. Park and K. L. Kim, *Appl. Catal., A*, 2000, **197**, 191.

51 C. H. Bartholomew, *Cat. Rev. Sci. Eng.*, 1982, **24**, 67.

52 J. Kopyscinski, T. J. Schildhauer and S. M. A. Biollaz, *Fuel*, 2010, **89**, 1763.

Table Captions:

Table 1. Physical properties of the supports and Ni catalysts.

Table 2. TPR quantitative data of the Ni catalysts.

Table 3. The XPS spectra results of catalyst supports.

Figure Captions:

Figure 1. XRD patterns of CTO and catalysts Ni/CTO (a), enlarged view zone of (b), and Al_2O_3 and catalysts Ni/Al_2O_3 (c), and TG/DTA curves of the CTO and Al_2O_3 supports (d).

Figure 2. H_2-TPR (a) and NH_3-TPD curves (b) of the supports and Ni catalysts, and H_2-TPD profile of the reduced Ni catalysts.

Figure 3. SEM images of the supports and the Ni catalysts before reduction: (a) CTO, (b) Al_2O_3, (c) 5Ni/CTO, (d) $5Ni/Al_2O_3$, (e) 10Ni/CTO, and (f) $10Ni/Al_2O_3$.

Figure 4. TEM images: (a and b) reduced 5Ni/CTO and Ni particles, (c and d) reduced 10Ni/CTO and Ni particles; (e and f) reduced $10Ni/Al_2O_3$ and Ni particles.

Figure 5. Ni 2p (a) and O 1s (b) XPS spectra of 5Ni/CTO, 10Ni/CTO and $10Ni/Al_2O_3$ catalysts after reduction.

Figure 6. Catalytic activities of the Ni catalysts at 0.1 MPa: (a) CO conversion, (b) CH_4 selectivity, and (c) CH_4 yield.

Figure 7. Catalytic activities of the Ni catalysts at 3.0 MPa: (a) CO conversion, (b) CH4 selectivity, and (c) CH4 yield.

Figure 8. Catalytic performance of the Ni catalysts for long time test at 600 ^{o}C and 3.0 MPa: (a) CO conversion, (b) CH_4 selectivity, and (c) CH_4 yield.

Figure 9. XRD patterns of reduced and used catalysts 10Ni/Al_2O_3 (a) and 10Ni/CTO (b), and SEM images of the used 10Ni/Al_2O_3 (c) and 10Ni/CTO (d).

Figure 10. Catalytic activities of the Ni catalysts after hydrothermal treatment: (a) CO conversion and (b) CH_4 yield.

Figure 11. Catalytic activities for CO_2 methanation: (a) CO_2 conversion and (b) CH_4 yield.

Table 1. Physical properties of the supports and Ni catalysts.

Catalyst Sample	BET surface area ($m^2 \cdot g^{-1}$)	Total pore volume ($m^3 \cdot g^{-1}$)	Mean particle size (nm)		
			NiO[a]	Ni[b]	Ni[c]
CTO	1.6	—	—	—	—
5Ni/CTO	2.9	—	19	16	10—20
10Ni/CTO	3.2	—	24	23	20—30
Al_2O_3	305.2	0.44	—	—	—
5Ni/Al_2O_3	268.5	0.37	—	—	3—5
10Ni/Al_2O_3	246.3	0.34	—	—	6—10

a: calculated by the XRD diffraction peak ($2\theta=47.9^{o}$) using Debye-Scherrer equation;

b: calculated by the XRD diffraction peak ($2\theta=43.5^{o}$) using Debye-Scherrer equation;

c: determined according to the TEM images.

Table 2. TPR quantitative data of the Ni catalysts.

Catalysts	T_m (^oC)			Fraction of total area (%)		
	α-type NiO	β-type NiO	γ-type NiO	α-type NiO	β-type NiO	γ-type NiO
5Ni/CTO	391	–	–	100	–	–
10Ni/CTO	384	–	–	100	–	–
5Ni/Al_2O_3	408	604	743	24.2	42.4	33.4
10Ni/Al_2O_3	351	588	739	12.0	53.5	34.4

Table 3. The XPS spectra results of catalyst supports.

Catalyst Sample	Binding Energy (eV)				
	Ca		Ti		Al
	Ca $2P_{3/2}$	Ca $2P_{1/2}$	Ti $2P_{3/2}$	Ti $2P_{1/2}$	Al 2P
5Ni/CTO	346.7	350	458.8	464.6	—
10Ni/CTO	346.4	350	458.6	464.3	—
10Ni/Al_2O_3	—	—	—	—	73.9

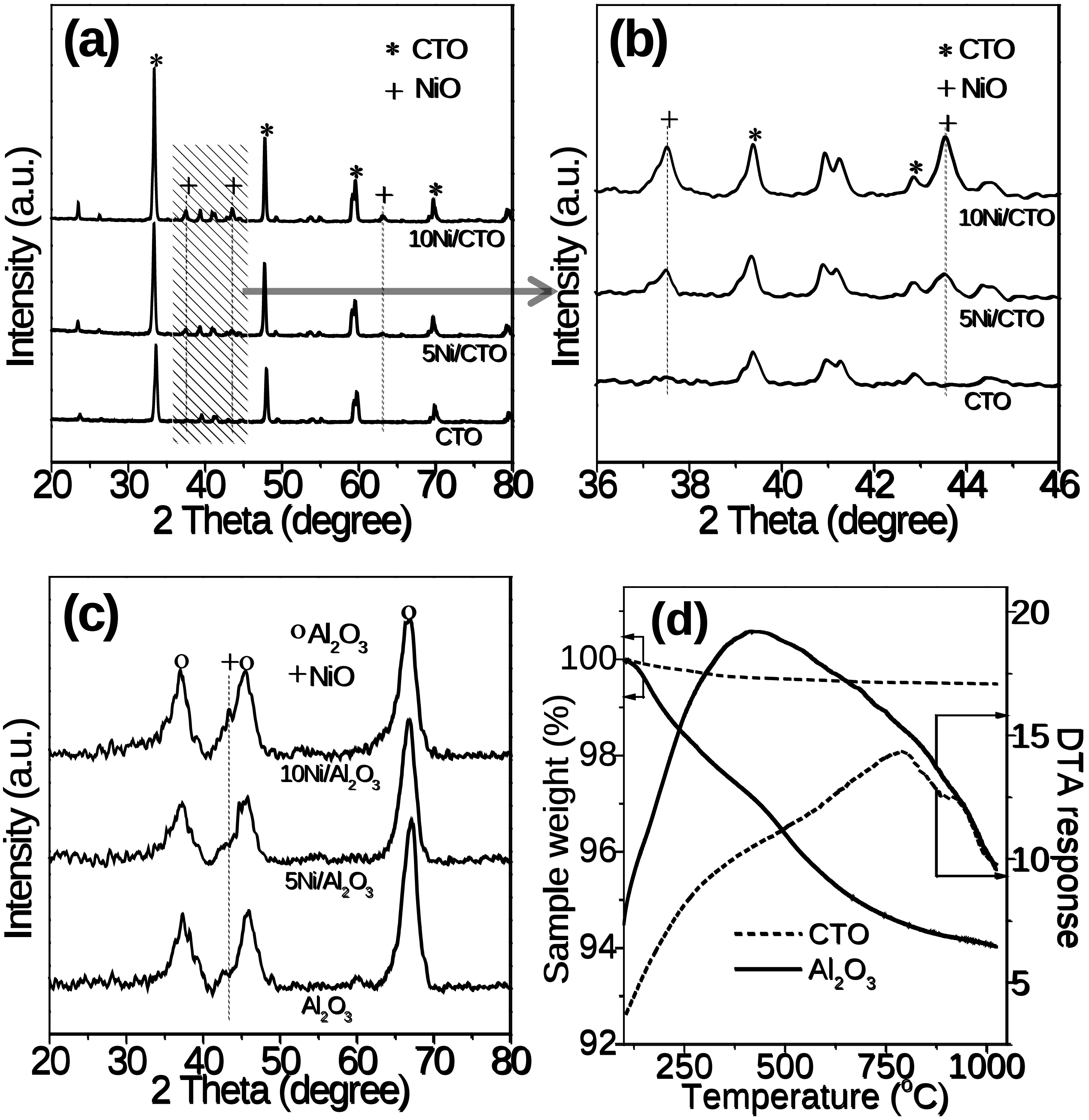

Figure 1. XRD patterns of CTO and catalysts Ni/CTO (a), enlarged view zone of (b), and Al_2O_3 and catalysts Ni/Al_2O_3 (c), and TG/DTA curves of the CTO and Al_2O_3 supports (d).

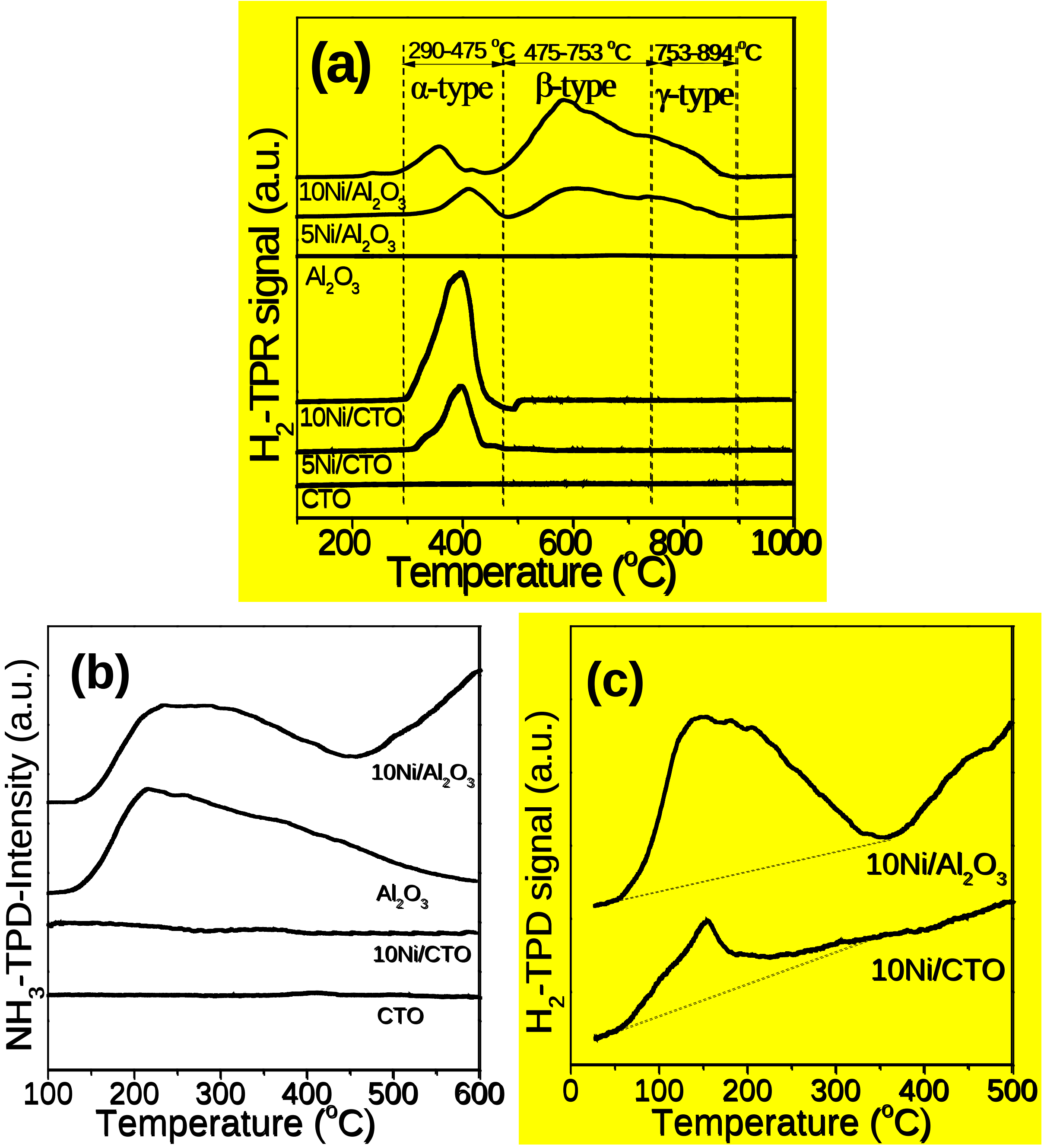

Figure 2. H_2-TPR (a) and NH_3-TPD curves (b) of the supports and Ni catalysts, and H_2-TPD profile of the reduced Ni catalysts.

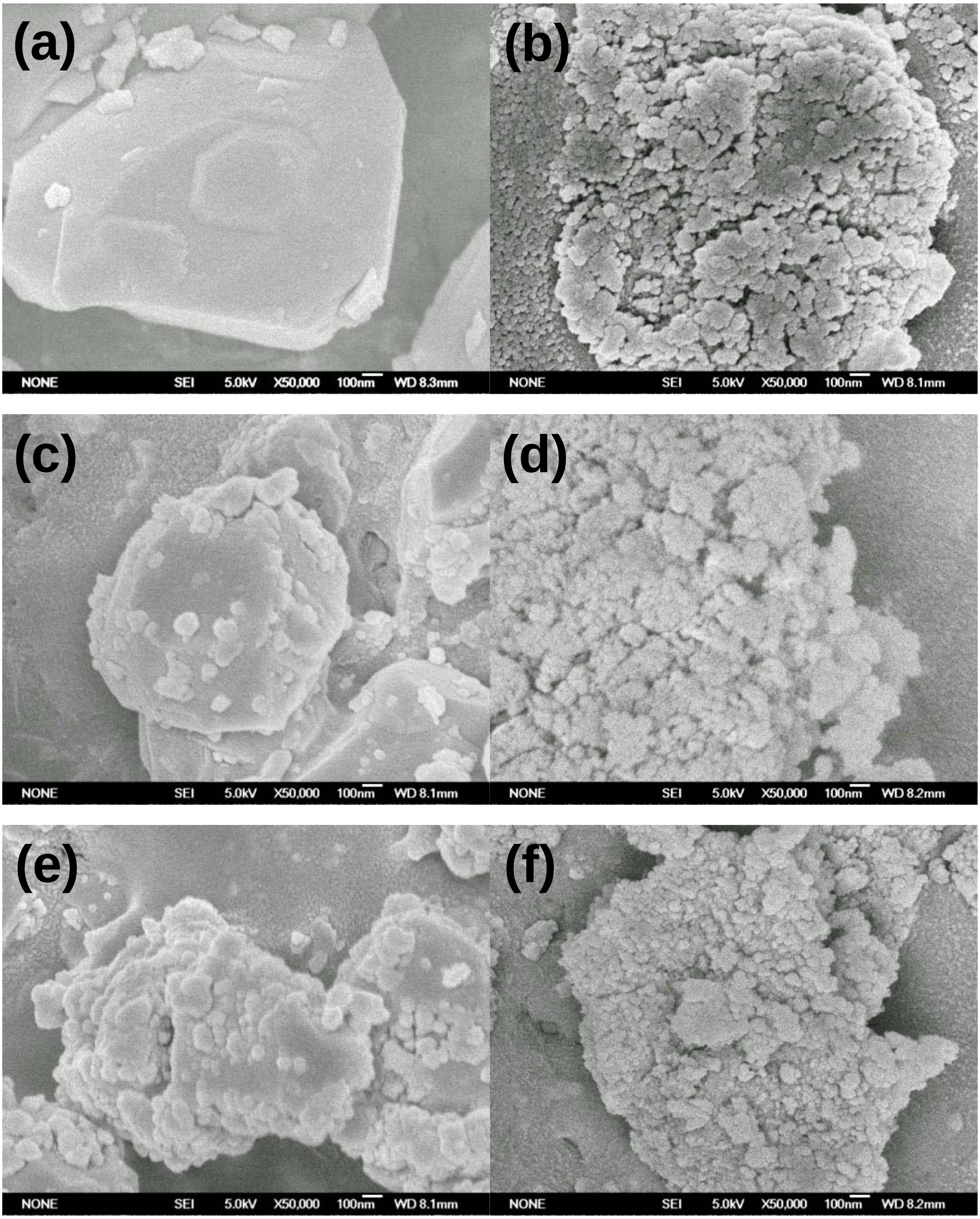

Figure 3. SEM images of the supports and the Ni catalysts before reduction: (a) CTO, (b) Al_2O_3, (c) 5Ni/CTO, (d) 5Ni/Al_2O_3, (e) 10Ni/CTO, and (f) 10Ni/Al_2O_3.

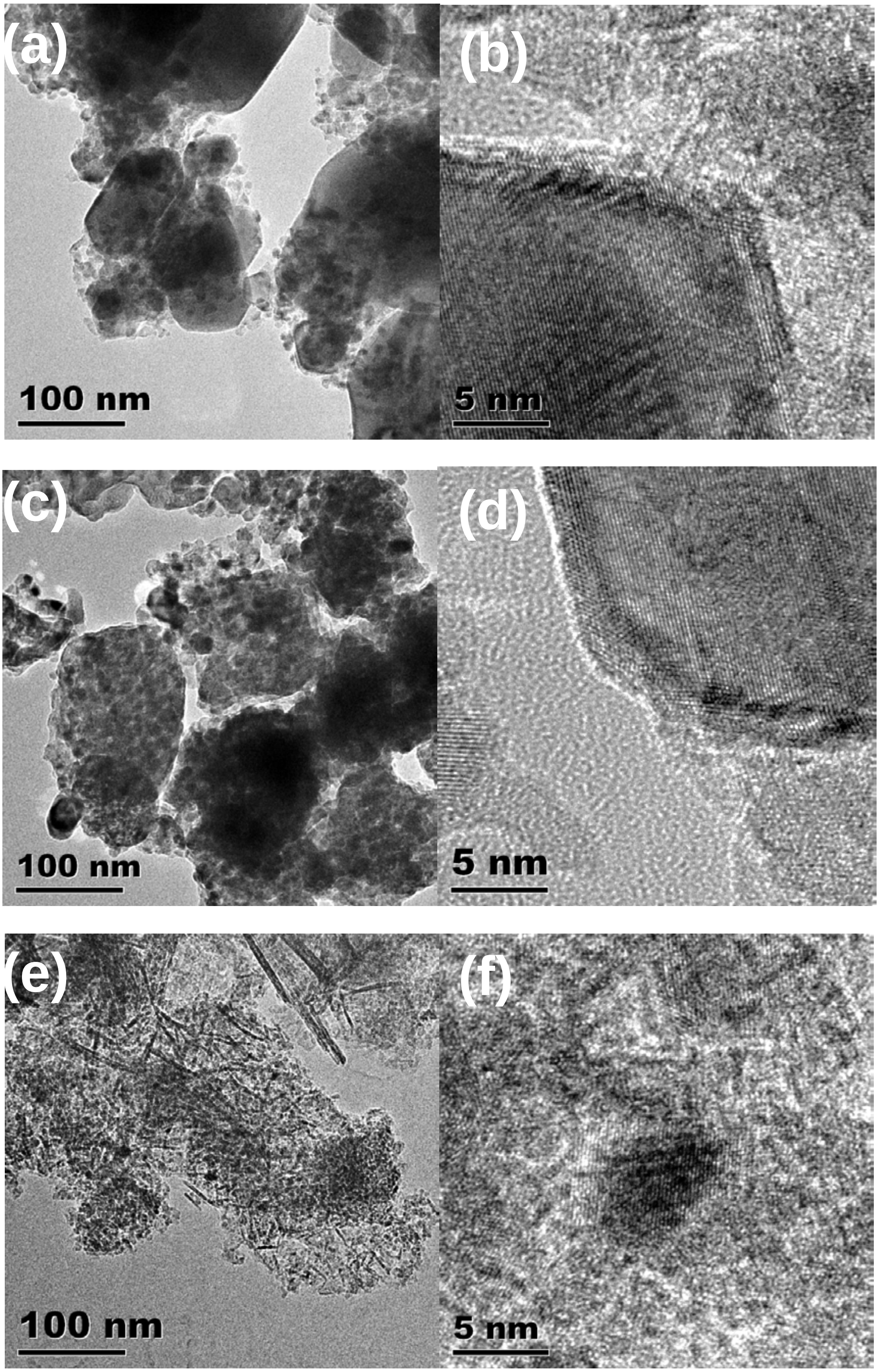

Figure 4. TEM images: (a and b) reduced 5Ni/CTO and Ni particles, (c and d) reduced 10Ni/CTO and Ni particles; (e and f) reduced 10Ni/Al_2O_3 and Ni particles.

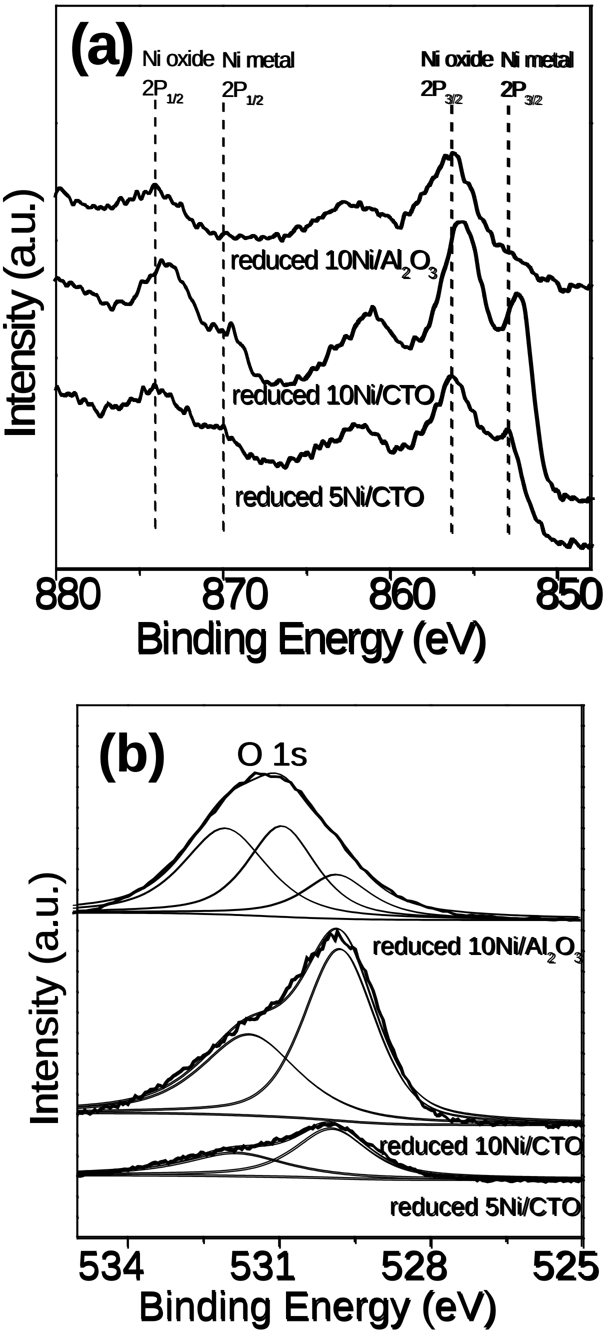

Figure 5. Ni 2p (a) and O 1s (b) XPS spectra of 5Ni/CTO, 10Ni/CTO and 10Ni/Al_2O_3 catalysts after reduction.

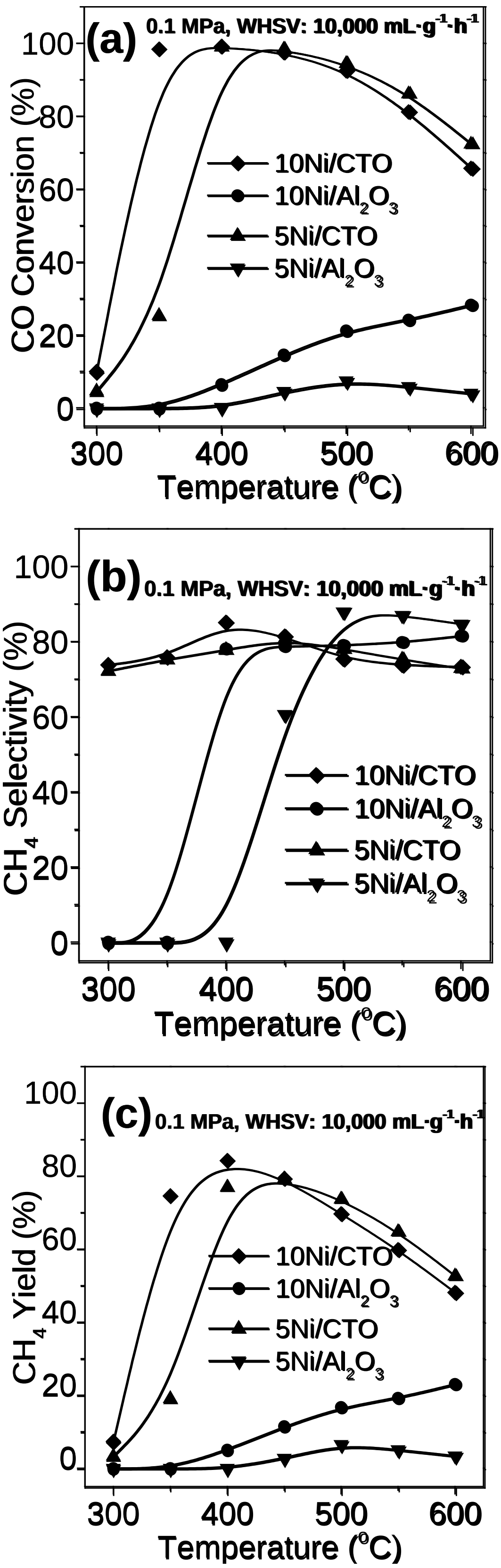

Figure 6. Catalytic activities of the Ni catalysts at 0.1 MPa: (a) CO conversion, (b) CH_4 selectivity, and (c) CH_4 yield.

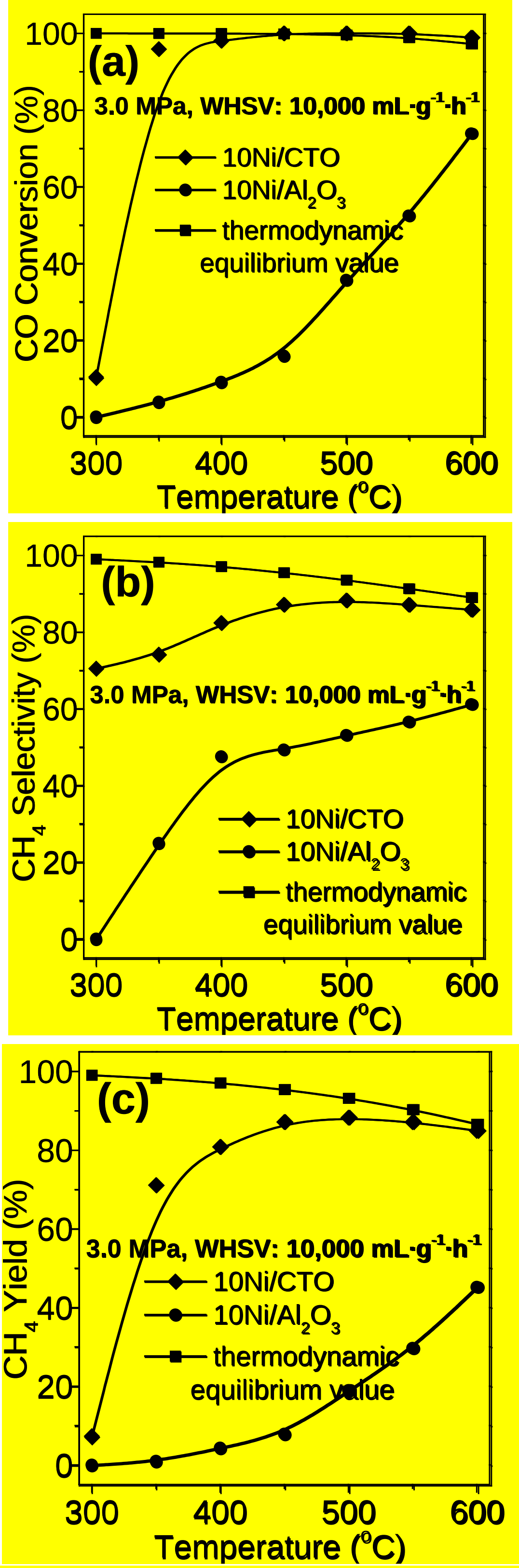

Figure 7. Catalytic activities of the Ni catalysts at 3.0 MPa: (a) CO conversion, (b) CH_4 selectivity, and (c) CH_4 yield.

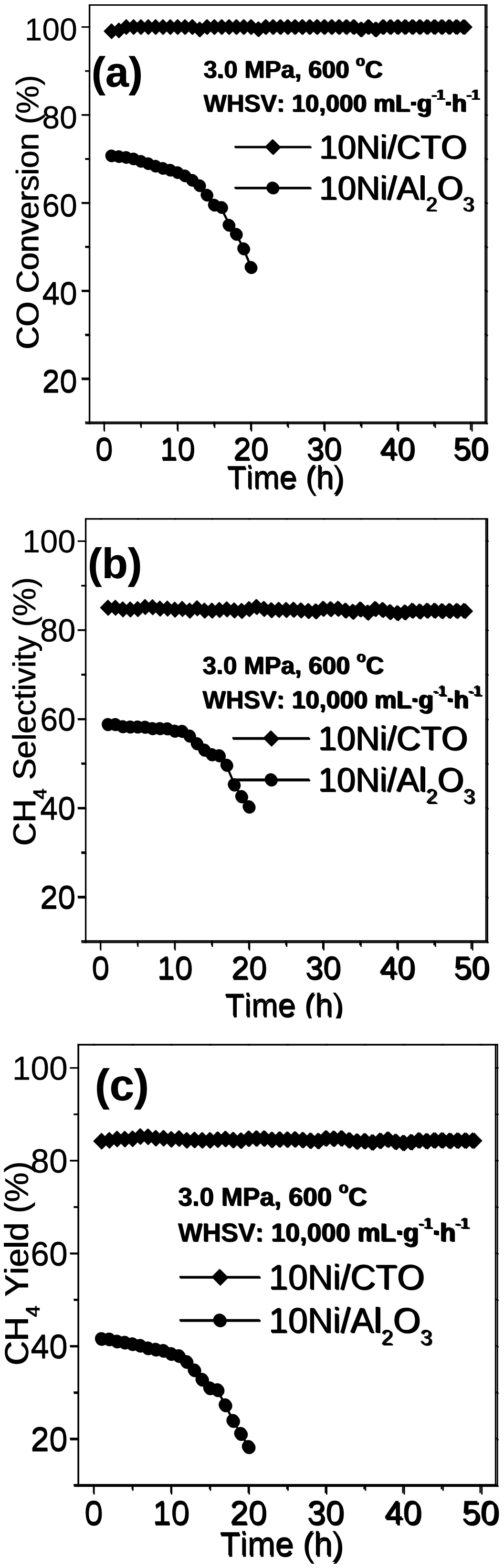

Figure 8. Catalytic performance of the Ni catalysts for long time test at 600 °C and 3.0 MPa: (a) CO conversion, (b) CH_4 selectivity, and (c) CH_4 yield.

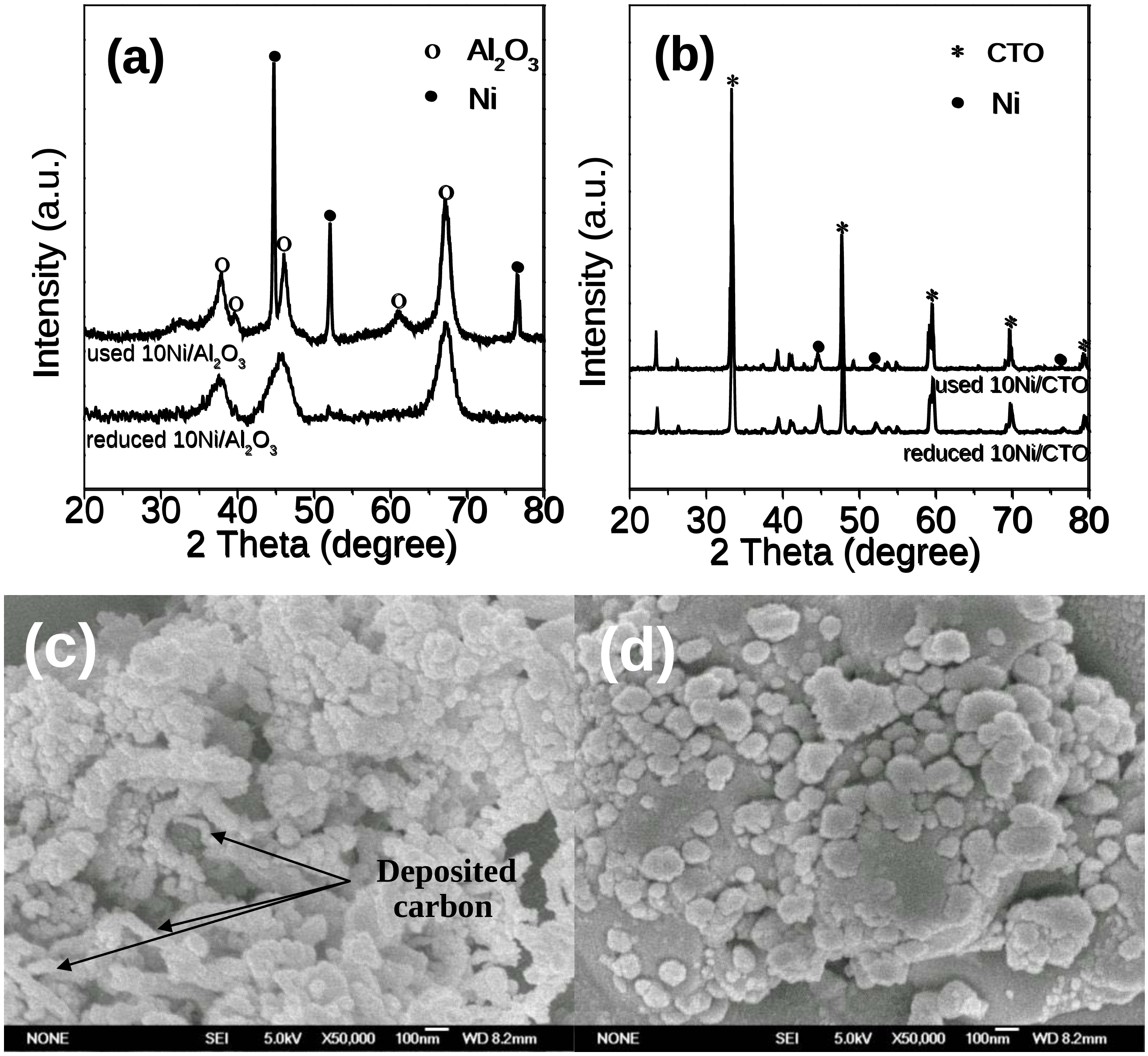

Figure 9. XRD patterns of reduced and used catalysts 10Ni/Al_2O_3 (a) and 10Ni/CTO (b), and SEM images of the used 10Ni/Al_2O_3 (c) and 10Ni/CTO (d).

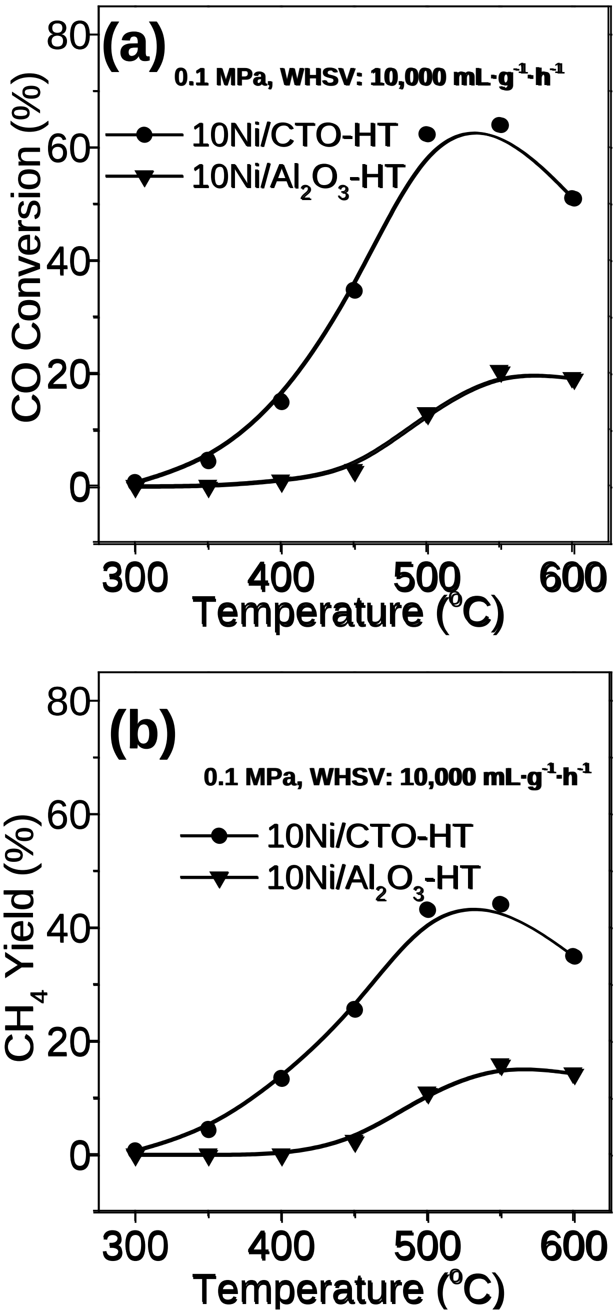

Figure 10. Catalytic activities of the Ni catalysts after hydrothermal treatment: (a) CO conversion and (b) CH_4 yield.

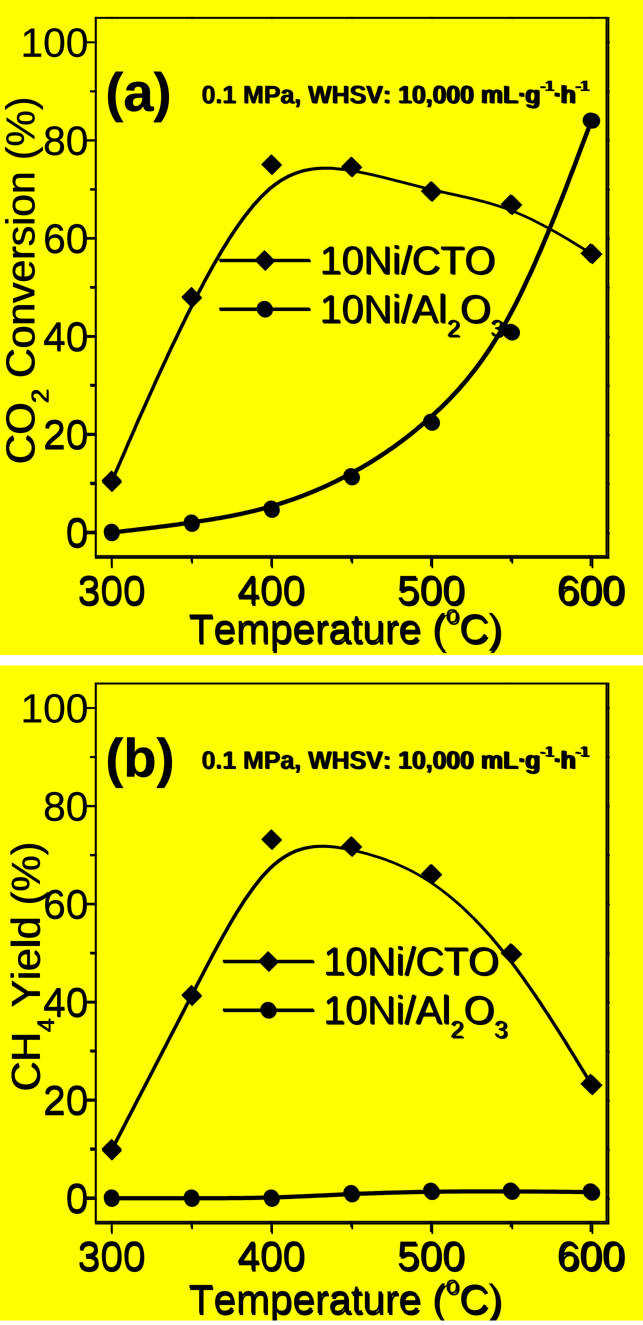

Figure 11. Catalytic activities for CO_2 methanation: (a) CO_2 conversion and (b) CH_4 yield.